Supporting Information

A Cobalt-Iron Double-Atom Catalyst for the Oxygen Evolution Reaction

Lichen Bai[1], Chia-Shuo Hsu[2], Duncan T. L. Alexander[3,4], Hao Ming Chen[2,*], and Xile Hu[1,*]

1. Laboratory of Inorganic Synthesis and Catalysis, Institute of Chemical Sciences and Engineering, Ecole Polytechnique Fédérale de Lausanne (EPFL), EPFL-ISIC-LSCI, BCH 3305, Lausanne, CH 1015 Switzerland.

2. Department of Chemistry, National Taiwan University, Taipei 10617, Taiwan

3. Interdisciplinary Centre for Electron Microscopy (CIME), Ecole Polytechnique Fédérale de Lausanne (EPFL), CH-1015 Lausanne, Switzerland

4. Electron Spectrometry and Microscopy Laboratory (LSME), Institute of Physics, Ecole Polytechnique Fédérale de Lausanne (EPFL), CH-1015 Lausanne, Switzerland

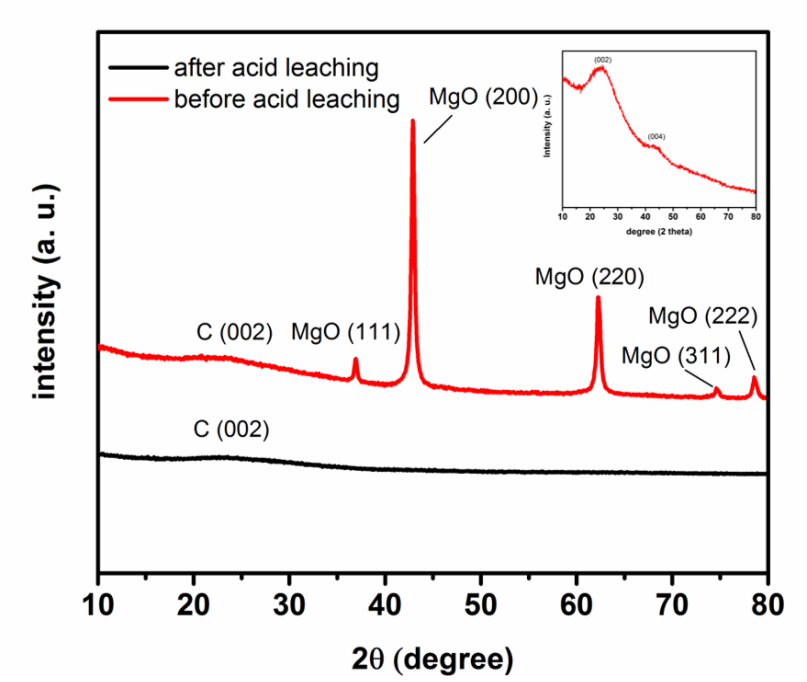

Figure S1. XRD of the as-prepared material and the material after acid leaching (Co-N-C). The inset is the magnified XRD pattern of the Co-N-C after acid leaching.

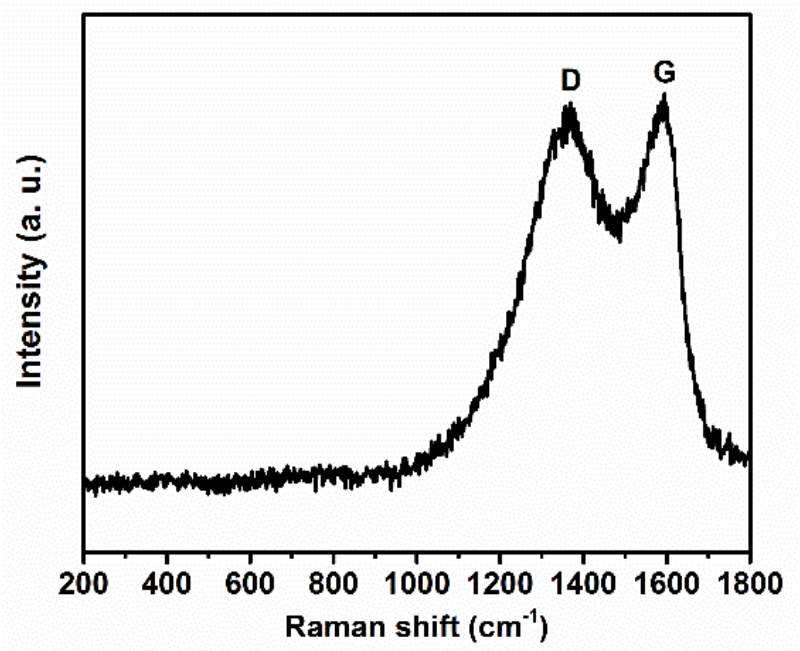

Figure S2. The Raman spectrum of Co-N-C calcinated at 700 ºC.

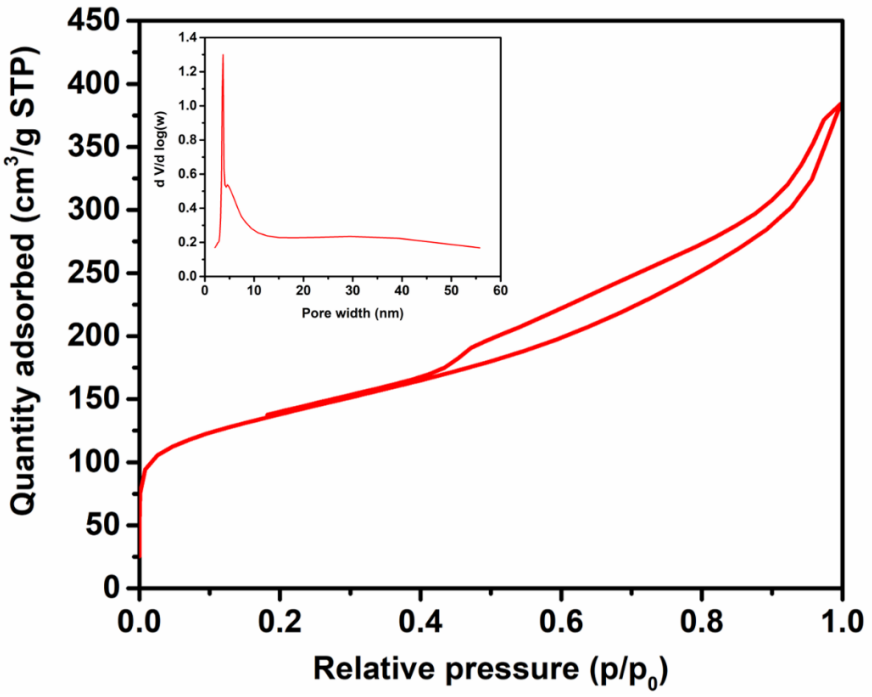

Figure S3. N_2 adsorption-desorption isotherms curve of Co-N-C. Inset is the curve of pore size distribution.

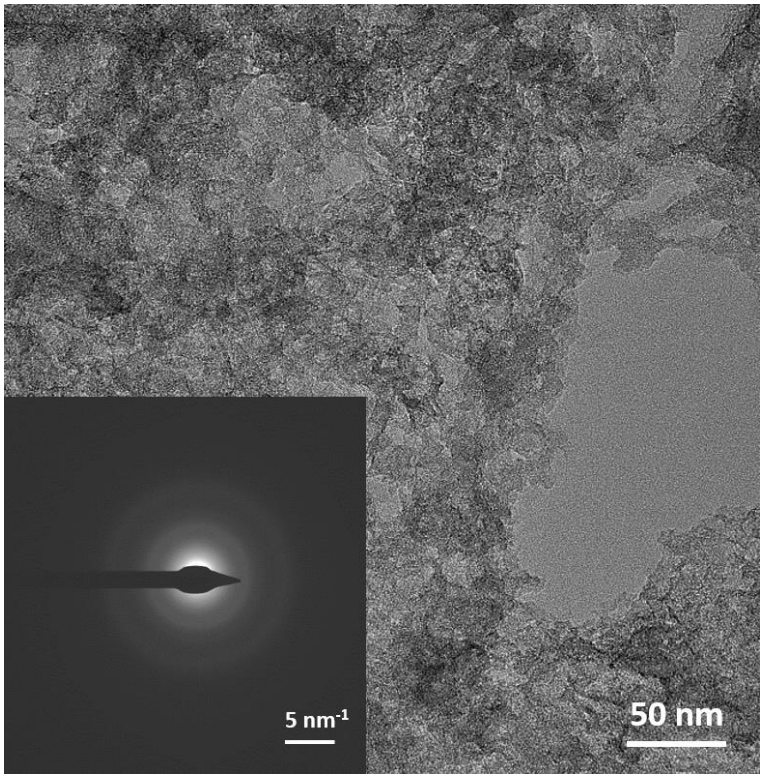

Figure S4. TEM image of Co-N-C; inset: the corresponding SAED pattern.

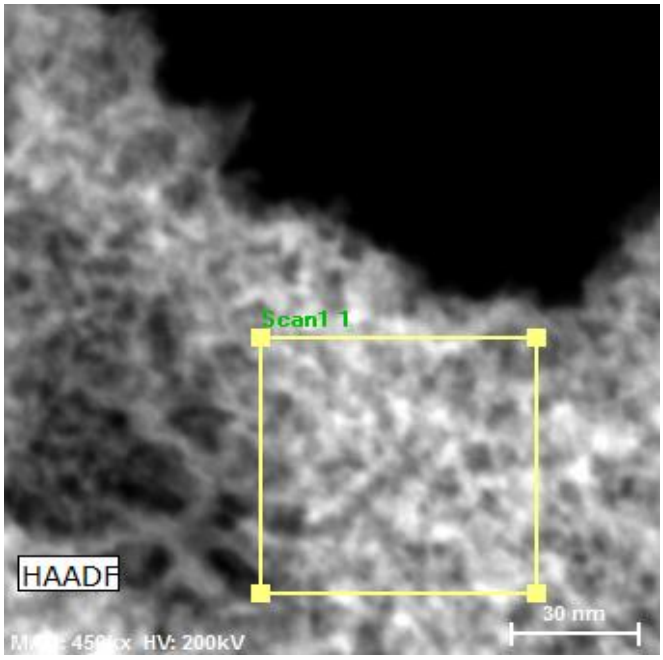

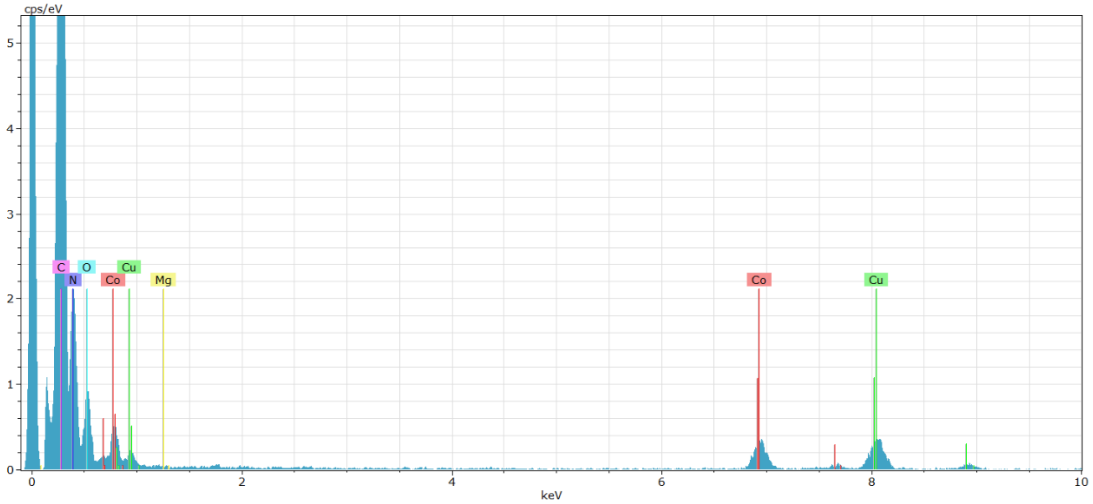

Figure S5. HAADF-STEM image of Co-N-C and the corresponding EDX spectrum from the indicated region. The Cu signals came from the Cu grid on which the sample was casted.

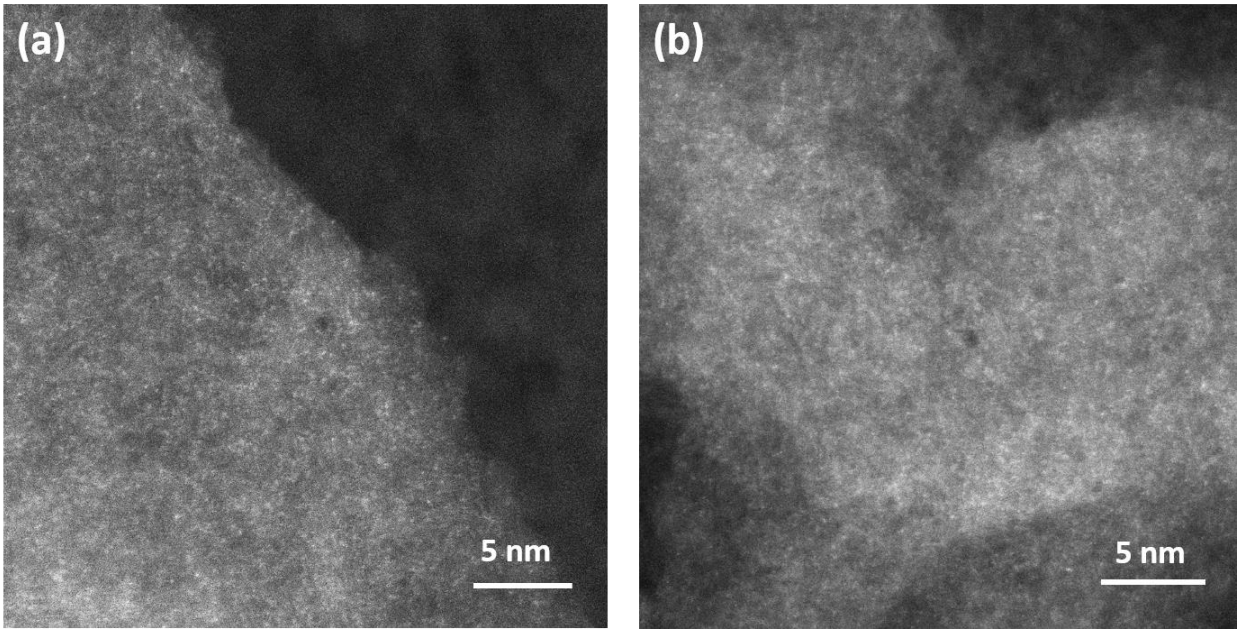

Figure S6. Additional spherical aberration-corrected HAADF-STEM images of Co-N-C.

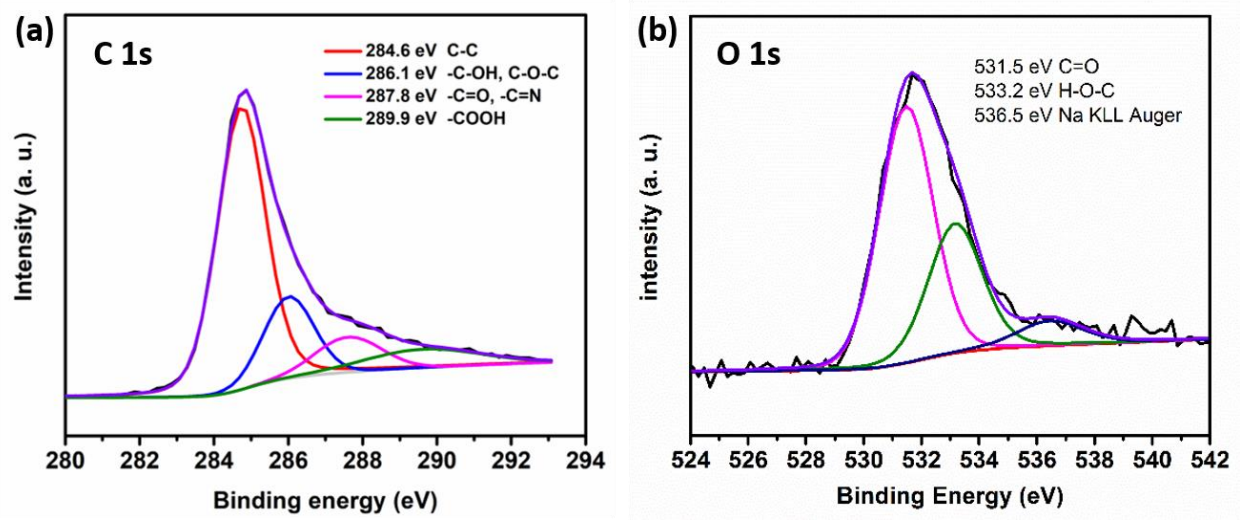

Figure S7. High resolution XPS of Co-N-C: (a) C 1s and (b) O 1s region.

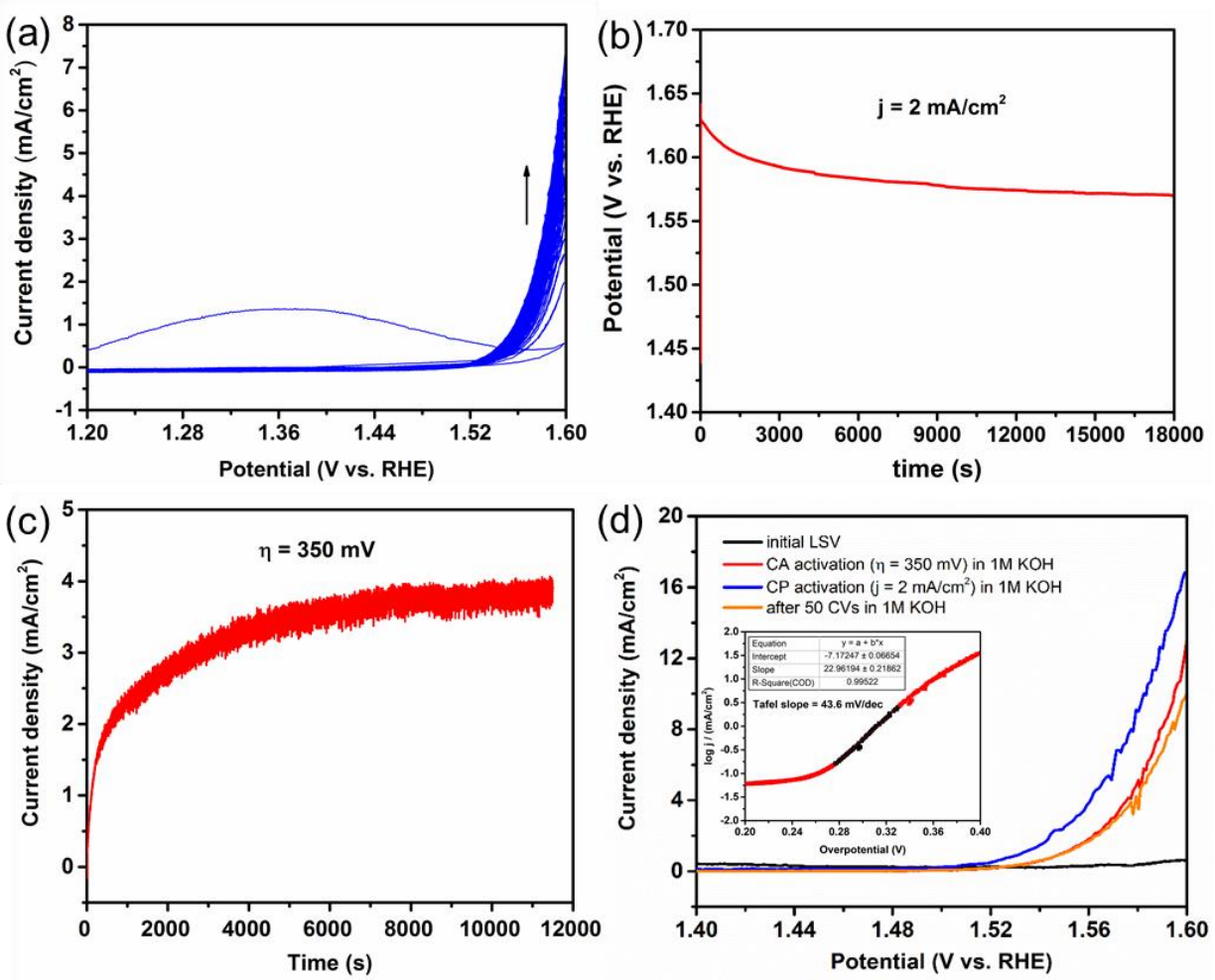

Figure S8. (a) Multiple CVs, (b) constant current activation process, and (c) constant potential activation process of Co-N-C. (d) Polarization curves of Co-N-C after activation. Inset: Tafel plot derived from polarization curve of Co-N-C activated by chronopotential method (blue line), the Tafel slope is 44 mV/dec. All the measurements were performed on a GC electrode.

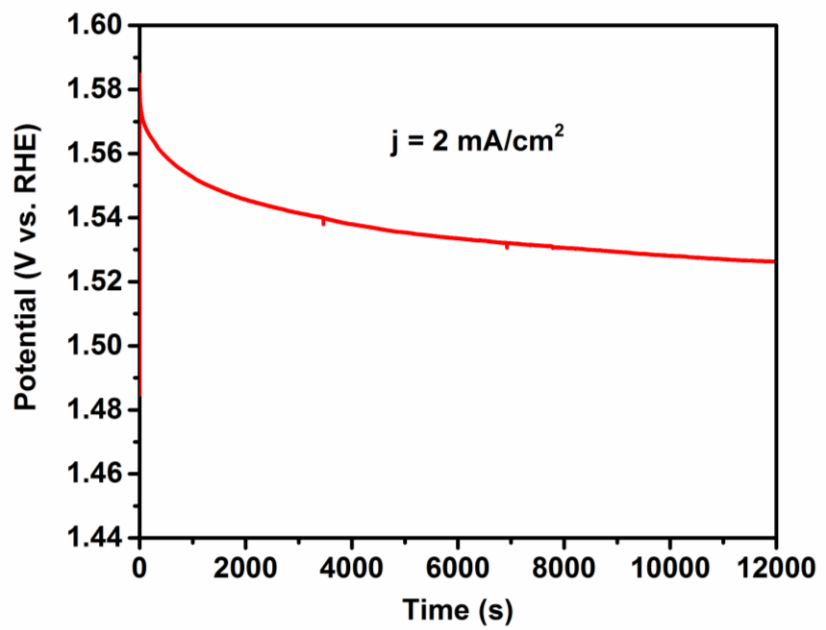

Figure S9. Constant current activation process of Co-N-C on a carbon-cloth electrode.

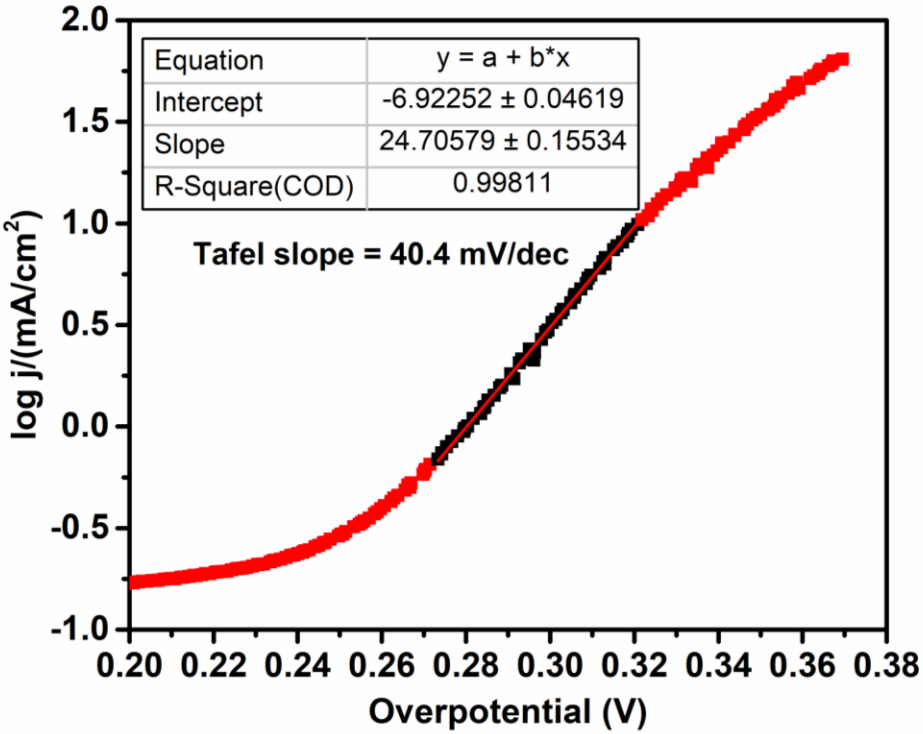

Figure S10. Tafel plot of Co-N-C on a carbon-cloth electrode after activation, the Tafel slope is 40 mV/dec.

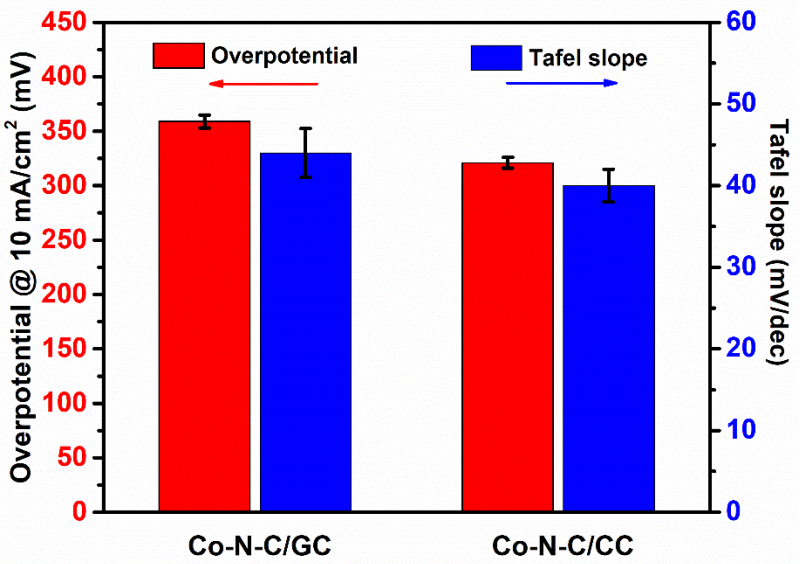

Figure. S11. Comparison of overpotential at the current density of 10 mA/cm^2 and Tafel slope for the activated Co-N-C modified on different electrode. GC = glassy carbon, CC = carbon-cloth.

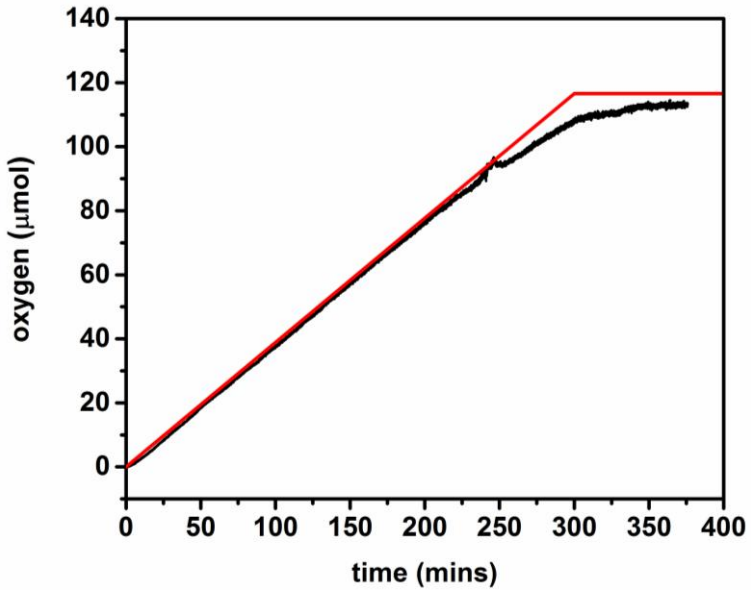

Figure S12. Oxygen evolution curve (black) of the activated Co-N-C (the red curve is the theoretical oxygen evolution curve assumed 100% Faradaic efficiency).

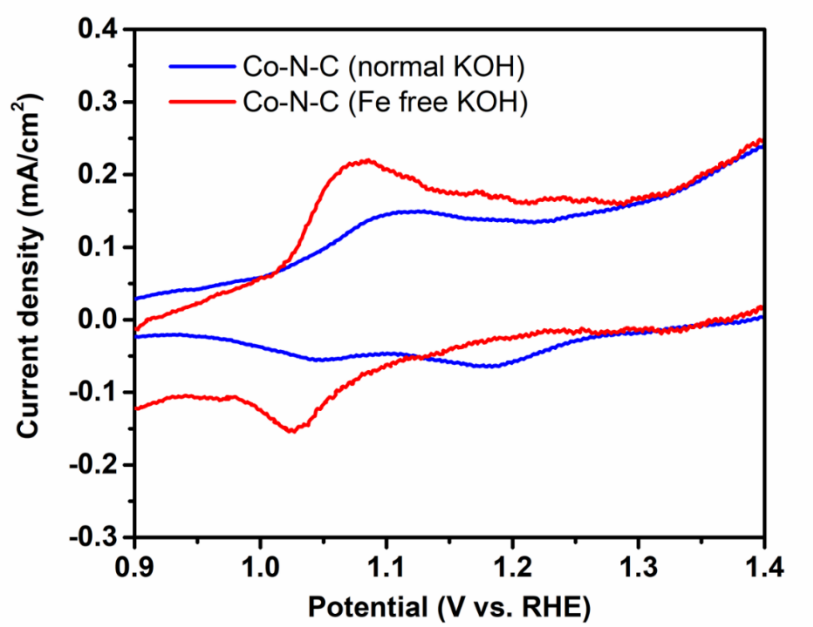

Figure S13. The CVs of Co-N-C after activated in normal KOH (Co-Fe-N-C, blue), $Ni(OH)_2$ treated KOH (Fe free, red).

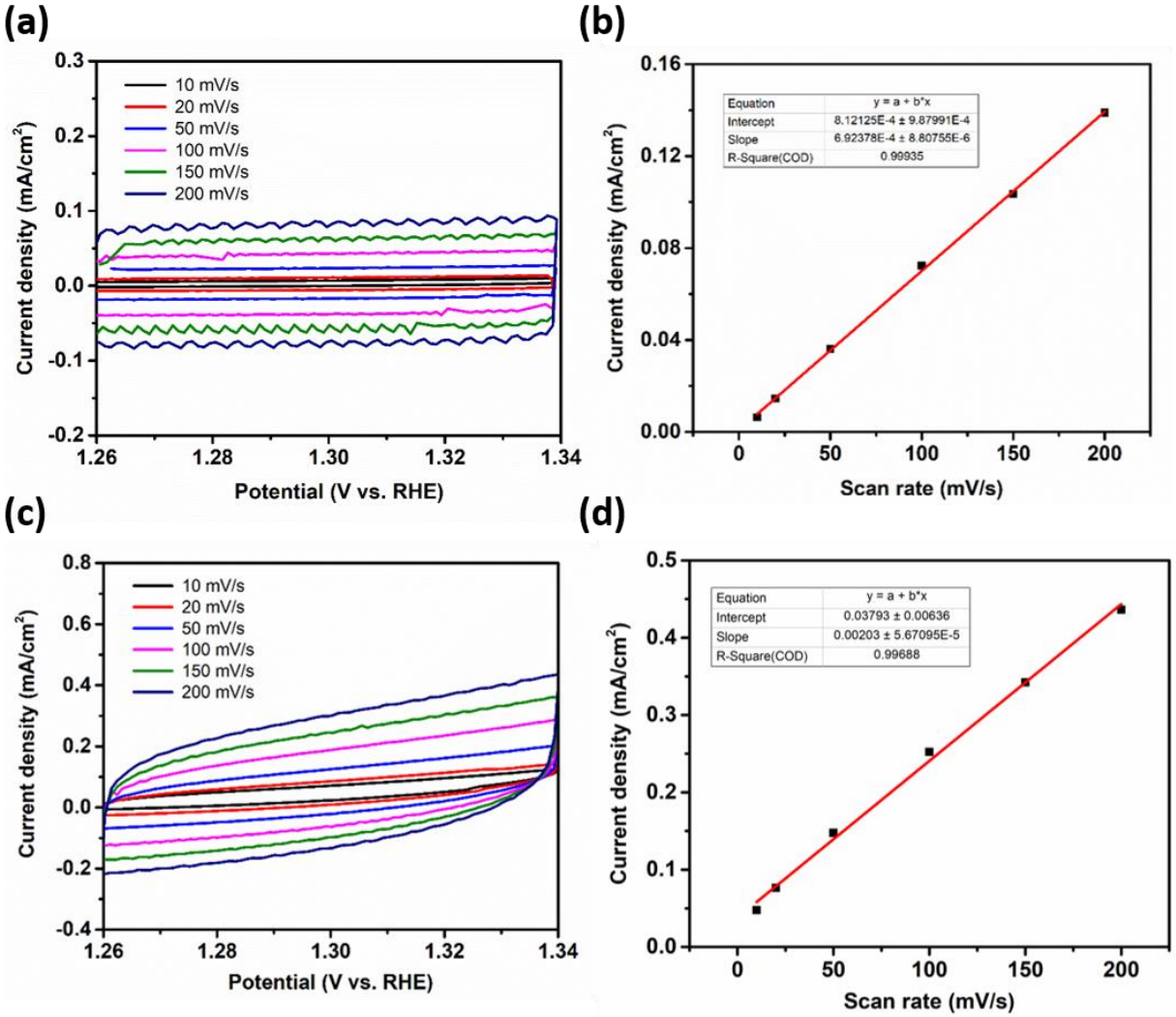

Figure S14. Measurements of double-layer capacitance of blank carbon-cloth electrode (CC) (a, b) and pristine Co-N-C on CC electrode (Co-N-C/CC) in Fe-free KOH (c, d). CVs from 1.26-1.34 V at different scan rates are shown for blank CC (a) and pristine Co-N-C/CC (c). The differences of current densities between charging and discharging process were plotted versus the scan rate for blank CC electrode (b) and pristine Co-N-C/CC (d). The calculated double-layer capacitance of blank CC and pristine Co-N-C/CC is 0.311±0.082 and 1.04±0.18 mF/cm^2, respectively. Therefore the ECSA of the pristine Co-N-C is 3.34±0.42 cm^2. The measurements were conducted on four different samples for each electrode.

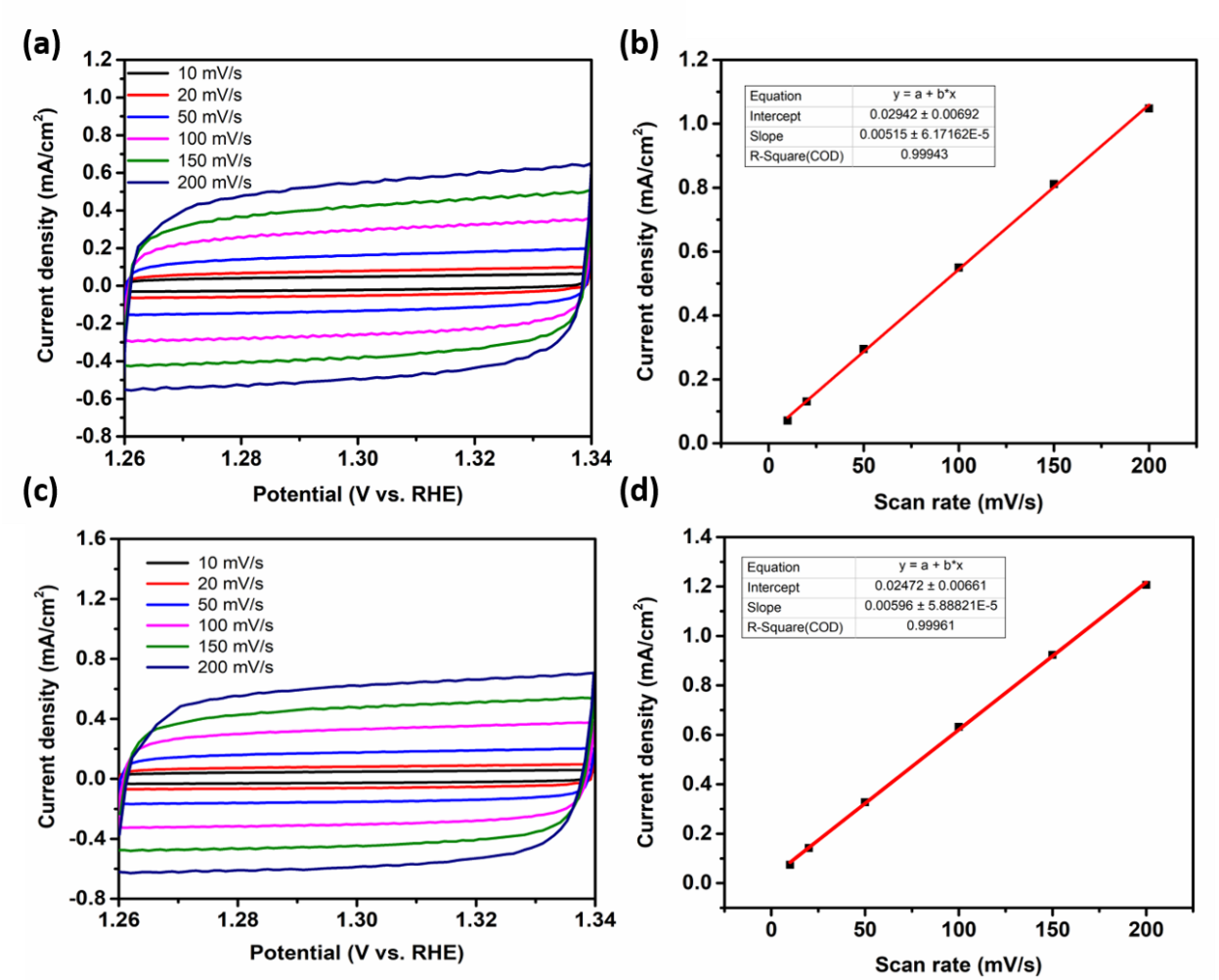

Figure S15. Measurements of double-layer capacitance of Co-N-C activated in Fe-free KOH (a, b) and Co-Fe-N-C (c, d) on CC electrodes. CVs from 1.26-1.34 V at different scan rate are shown for Co-N-C activated in Fe-free KOH (a) and Co-Fe-N-C (c). The differences of current densities between charging and discharging process were plotted versus the scan rate for Co-N-C activated in Fe-free KOH (b) and Co-Fe-N-C (d). The calculated double-layer capacitance of Co-N-C activated in Fe-free KOH and Co-Fe-N-C is 2.60±0.27 and 3.20±0.47 mF/cm^2, respectively. Therefore the ECSA of the Co-N-C activated in Fe-free KOH and the Co-Fe-N-C is 8.36±1.84 and 10.29±1.11 cm^2, respectively. The measurements were conducted on four different samples for each electrode.

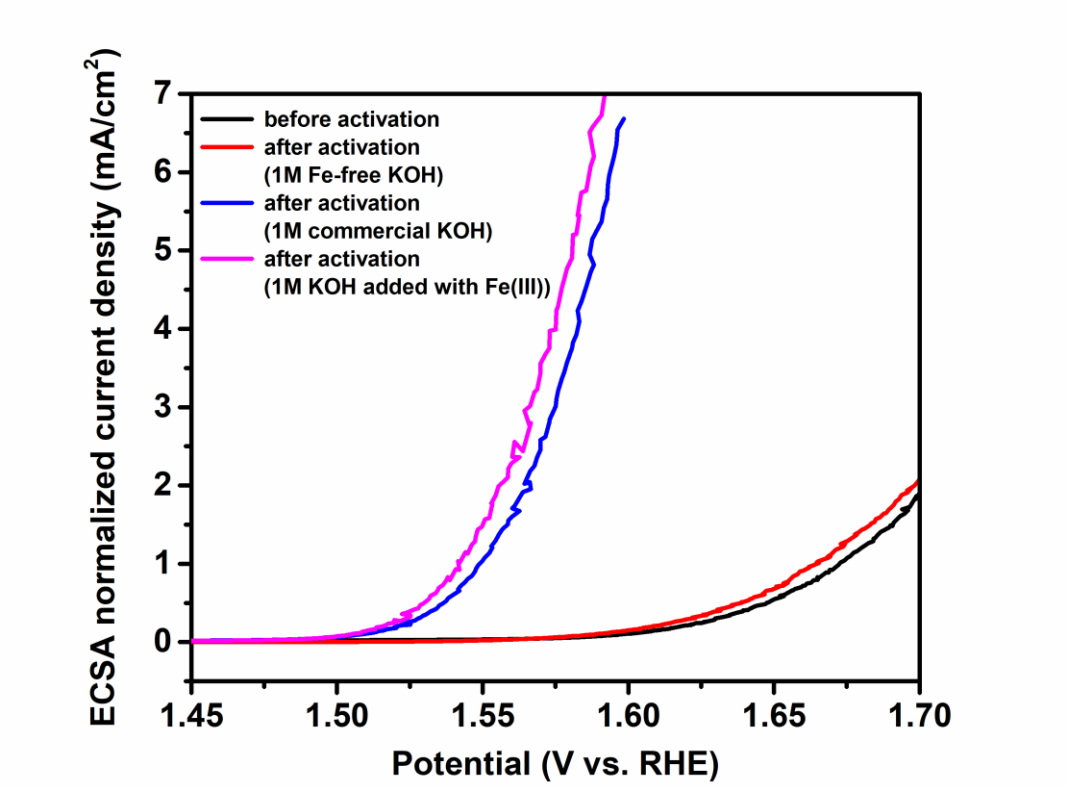

Figure S16. ECSA-normalized activity of pristine Co-N-C (black), Co-N-C activated in Fe-free KOH (red), in normal KOH (blue) and Fe(III)-added KOH (pink).

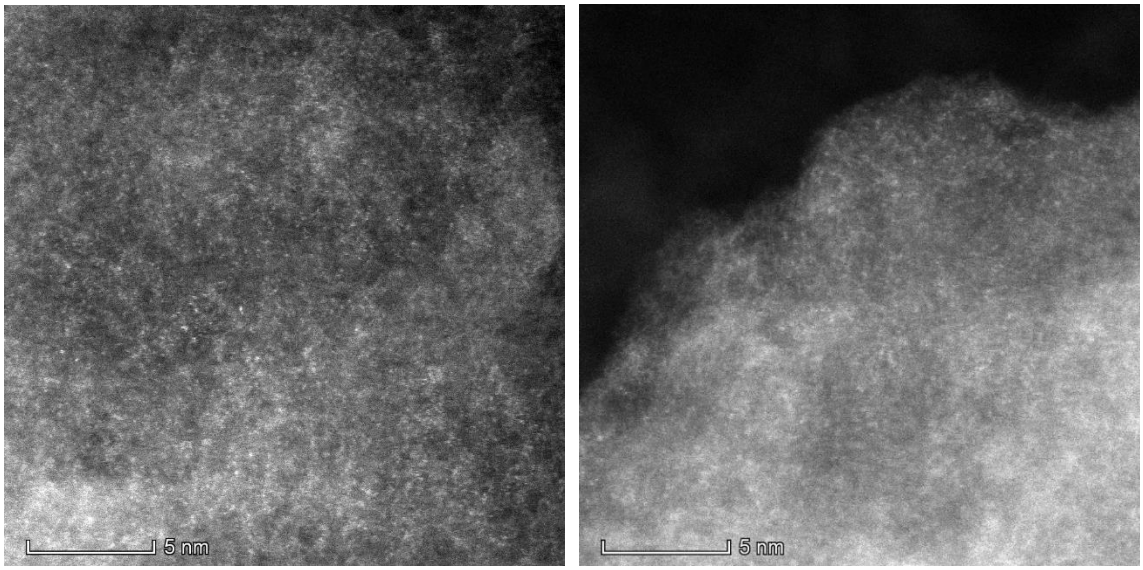

Figure S17. Additional aberration-corrected HAADF-STEM images of Co-Fe-N-C.

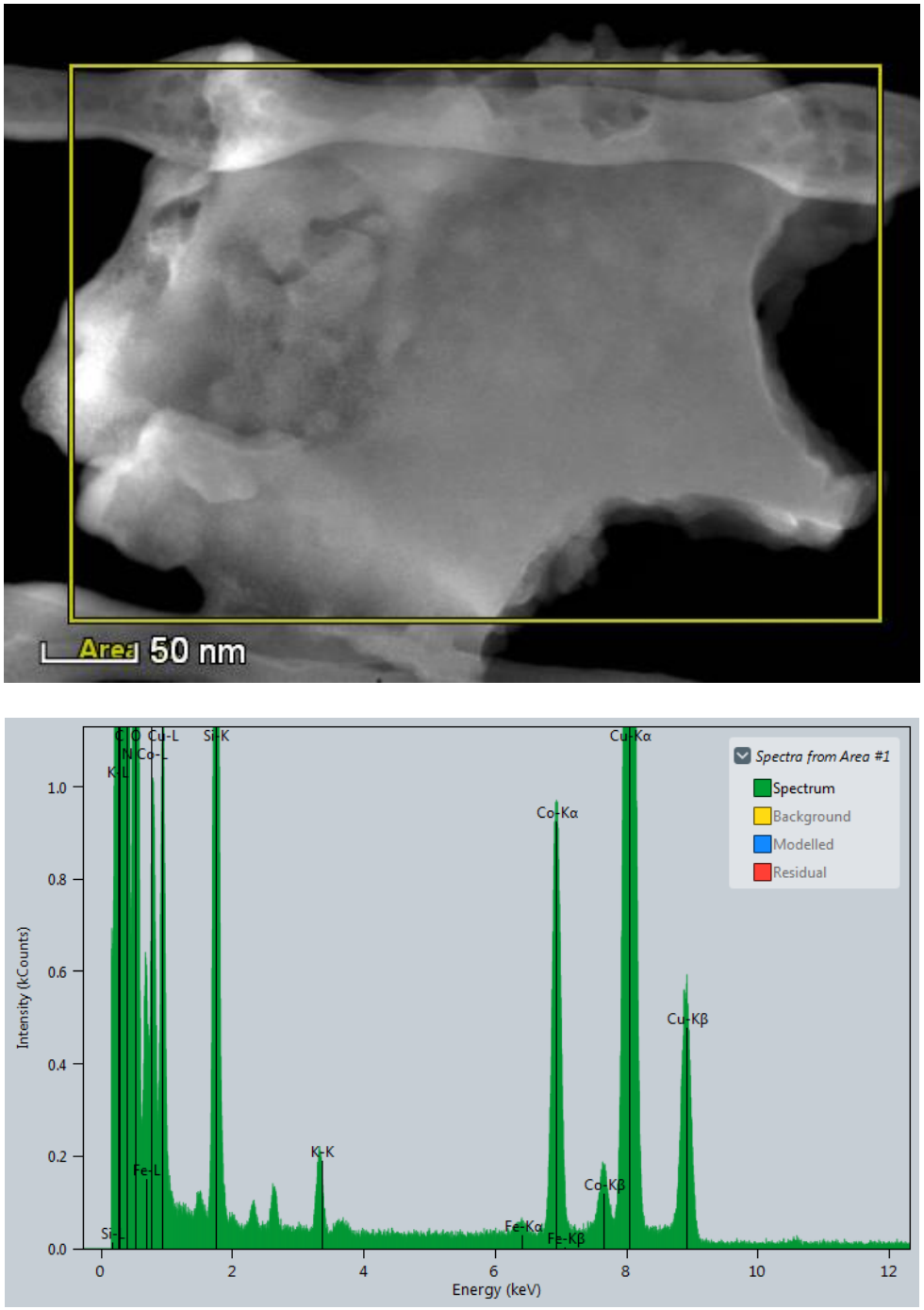

Figure S18. Upper: HAADF-STEM image of Co-Fe-N-C (Fig. 3c in main text) and bottom: EDX spectrum of indicated region in the HAADF-STEM image. The Cu signals came from the Cu grid on which the sample was casted.

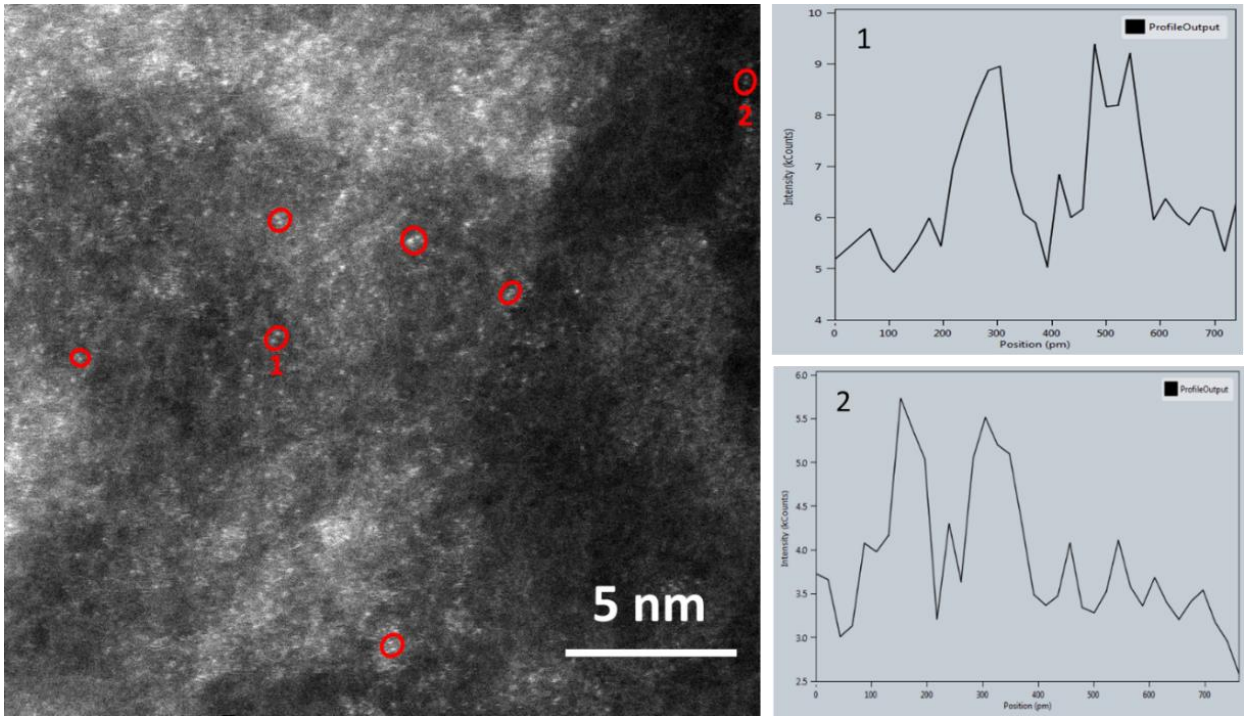

Figure S19. Analysis of a typical aberration-corrected HAADF-STEM image of Co-Fe-N-C (Fig. 3b in the maintext). Some closely-located atom pairs are marked with red circles. The intensity profiles (e.g., for 1 and 2) indicate that they are possibly Co-Fe dimers. (The HAADF intensity of each atom would be very similar because of their neighboring atomic numbers.)

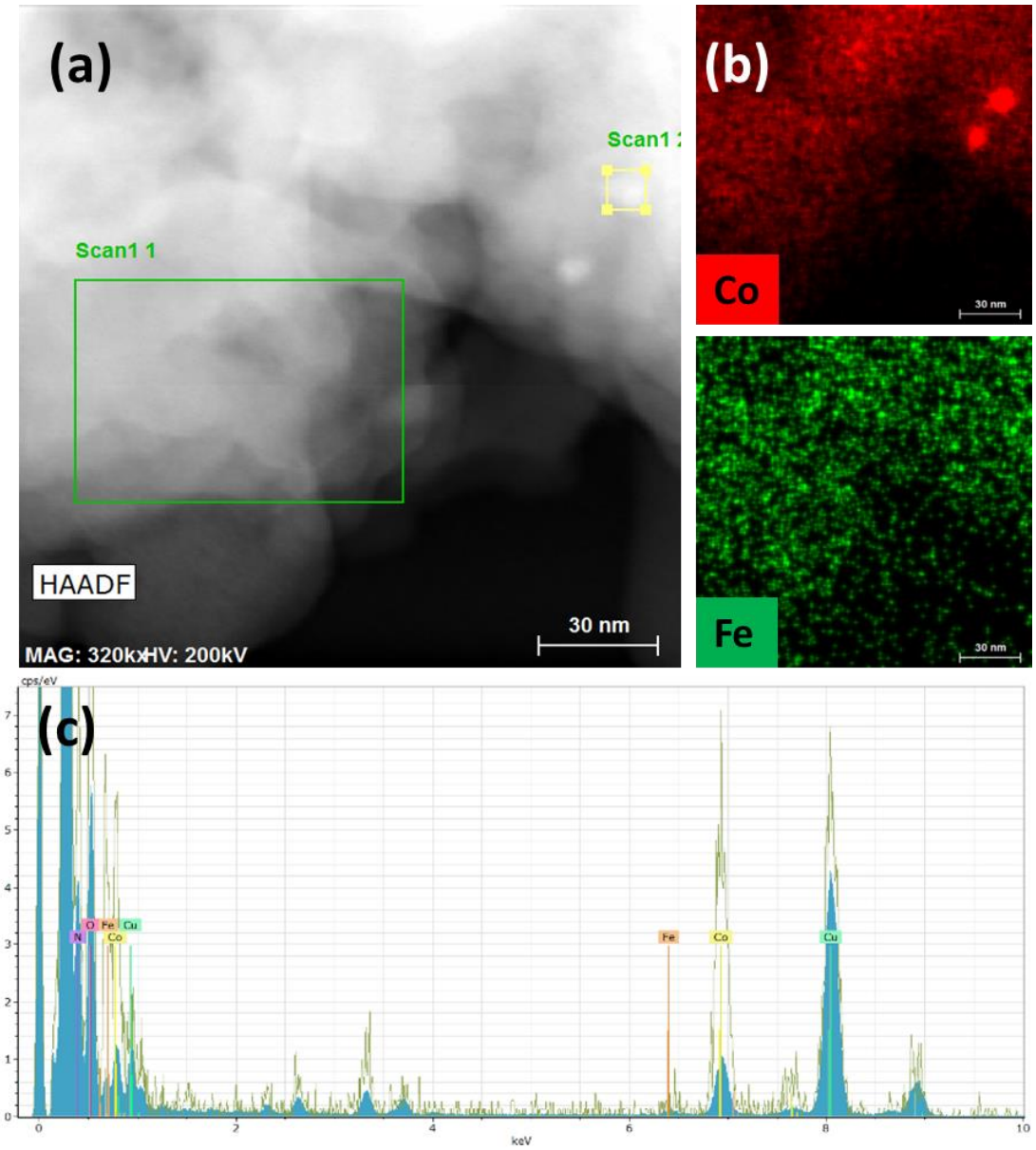

Figure S20. (a) HAADF-STEM image, (b) elemental EDXS mapping and (c) EDX spectra of Co-Fe-N-C from an area that contained nanoparticles. The spectra showed that the content of Co is higher for the region containing a nanoparticle (1-2) but the content of Fe is similar to the area without nanoparticles (1-1). The Cu signals came from the Cu grid on which the sample was casted.

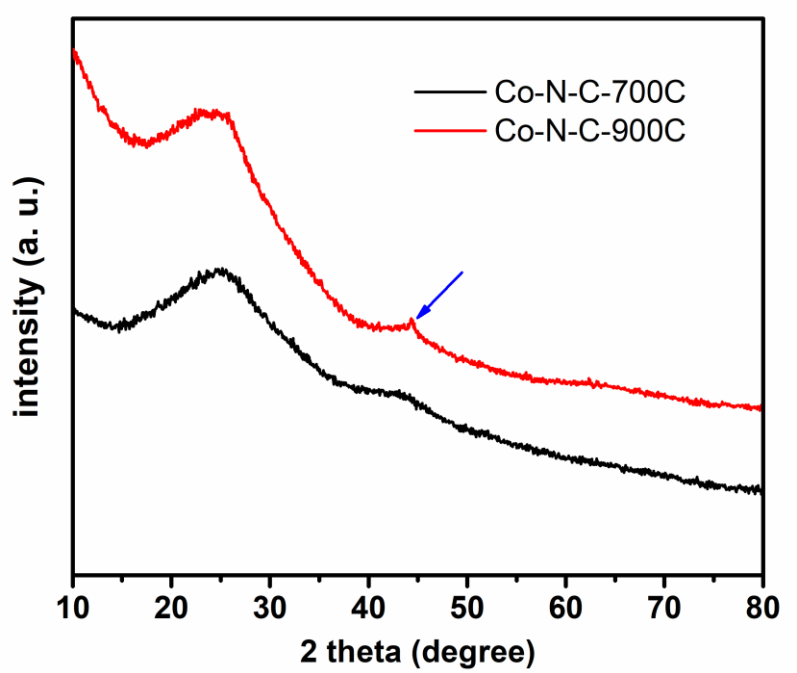

Figure S21. XRD of Co-N-C calcinated at different temperatures. The blue arrow indicated the diffraction peak of (111) facet of metallic Co (Reference code: 00-015-0806).

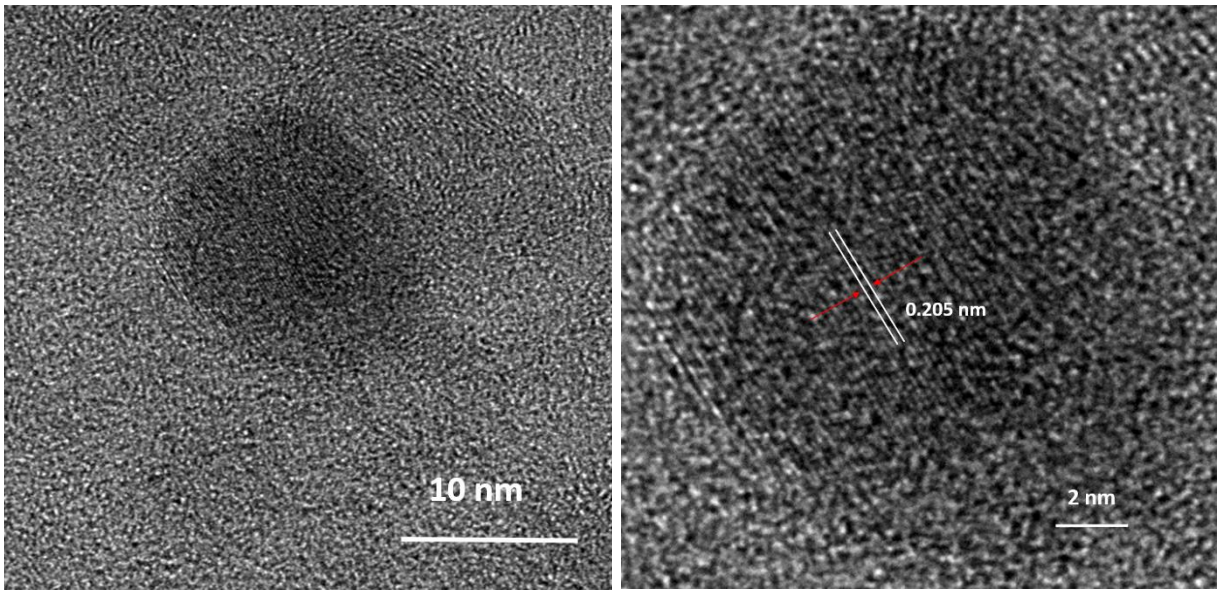

Figure S22. HR-TEM image of Co-N-C-900C. The marked distance of the lattice fringes corresponds to (111) planes of metallic Co (Reference code: 00-015-0806).

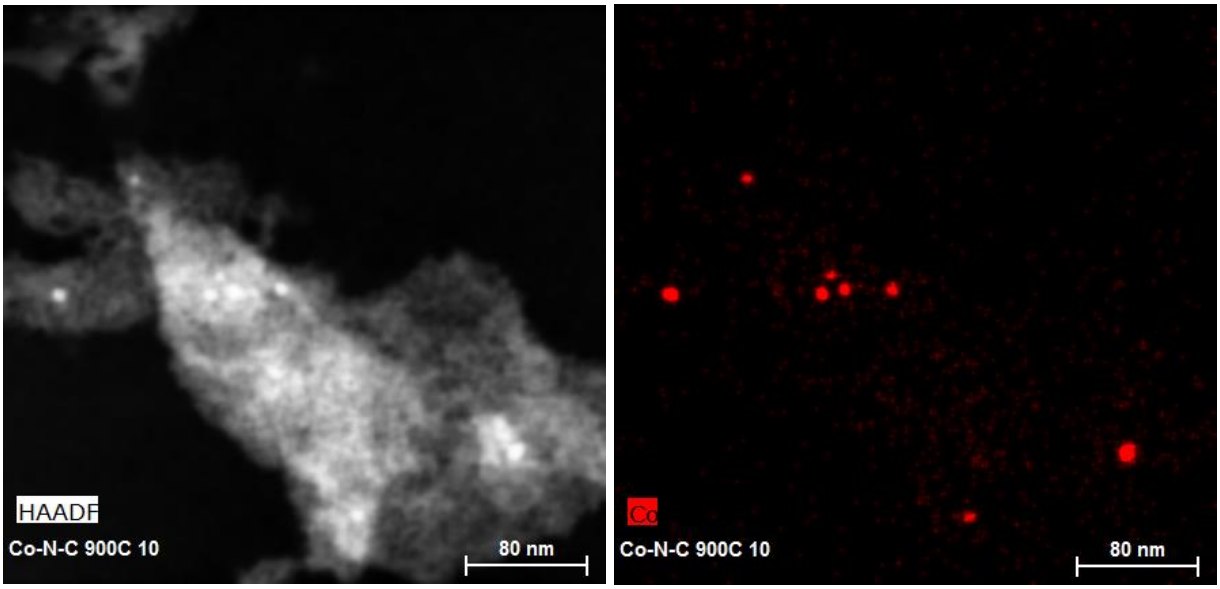

Figure S23. HAADF STEM images and the corresponding EDXS mapping of Co for Co-N-C-900.

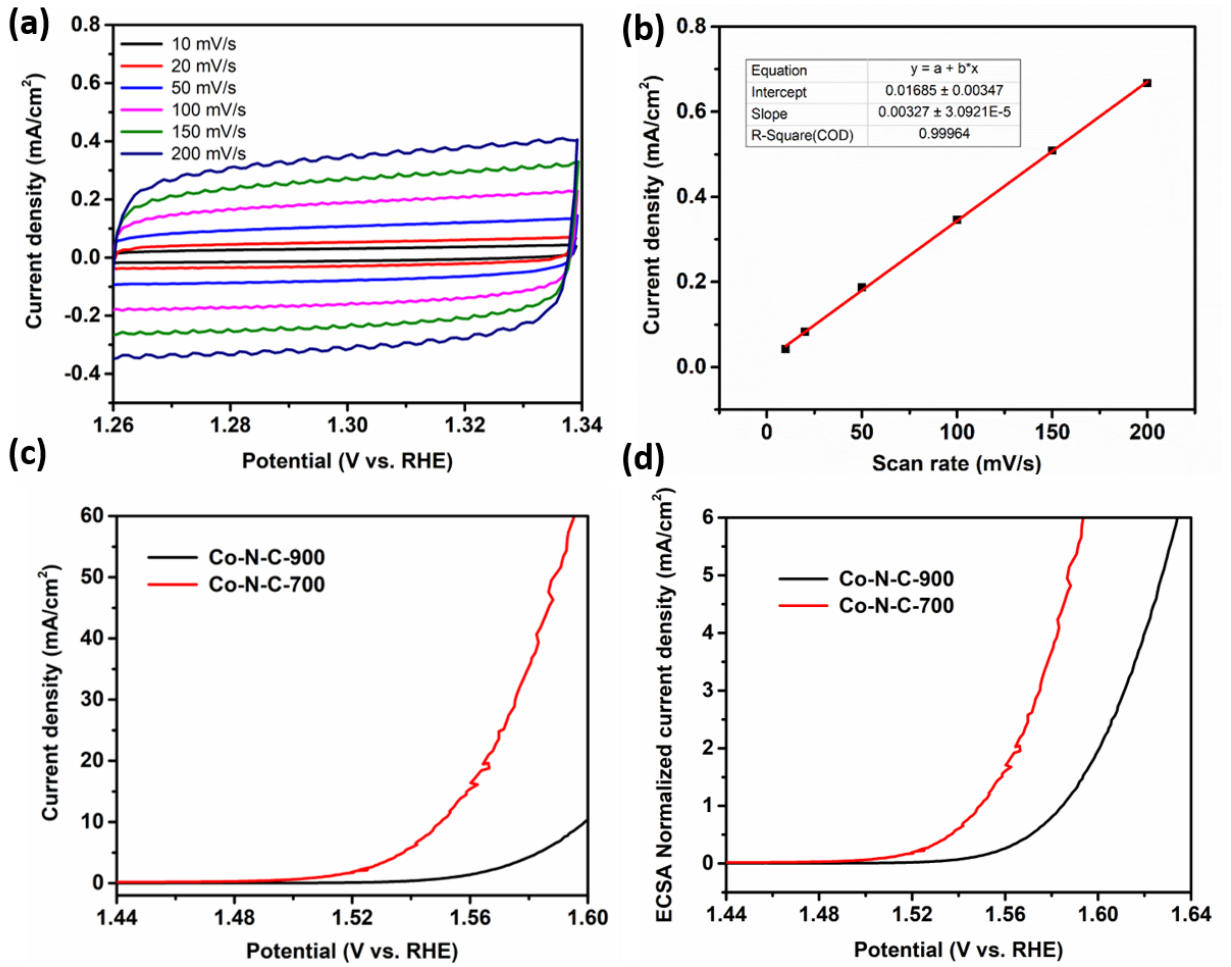

Figure S24. (a, b) Measurements of double-layer capacitance of Co-N-C-900 after activation in normal KOH. (a) CVs from 1.26-1.34 V at different scan rates; (b) The differences of current densities between charging and discharging process were plotted versus the scan rates. The calculated double-layer capacitance of activated Co-N-C-900 is 1.65±0.14 mF/cm^2. Therefore the ECSA of the activated Co-N-C-900 is 5.30±1.30 cm^2. The measurements were conducted on four different samples (c) LSVs and (d) ECSA-normalized LSVs of Co-N-C calcinated at different temperature after activation in normal KOH.

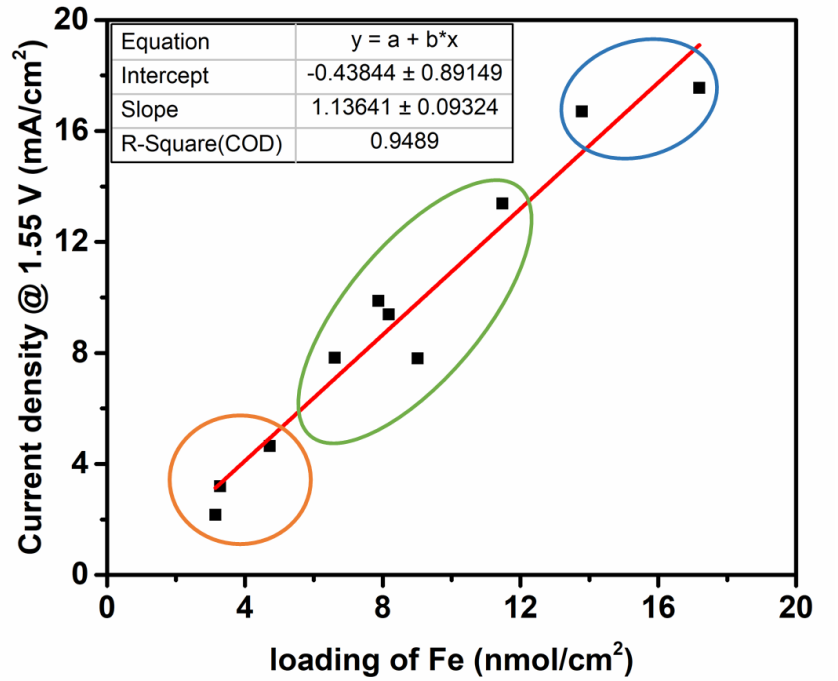

Figure S25. The current density at 1.55 V vs. RHE for the catalysts with different Fe loadings. The circles with different colors pointed the samples activated in different electrolyte. Orange: activated in 1M KOH for 2h. Green: activated in 1M KOH until stabilized performance. Blue: activated in 1M KOH added with 10 ppm Fe^{3+} until stabilized performance.

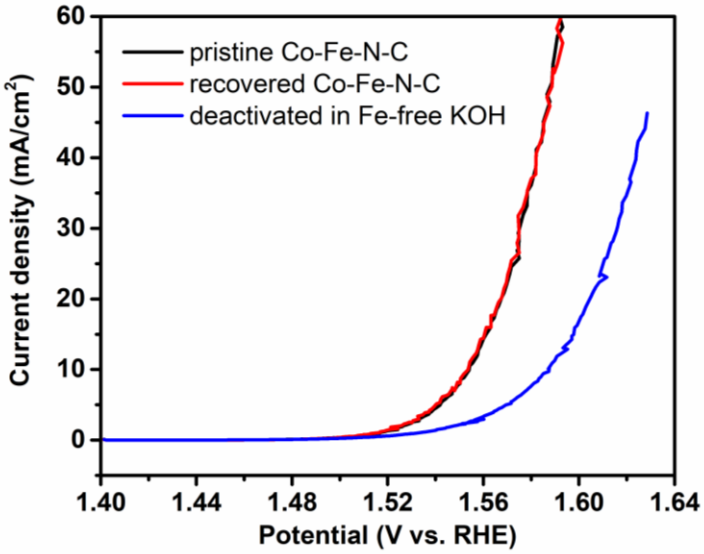

Figure S26. LSVs of Co-Fe-N-C before and after electrolysis in 1M Fe free KOH for 2h. The activity can be recovered by re-activating the catalyst in fresh 1M KOH.

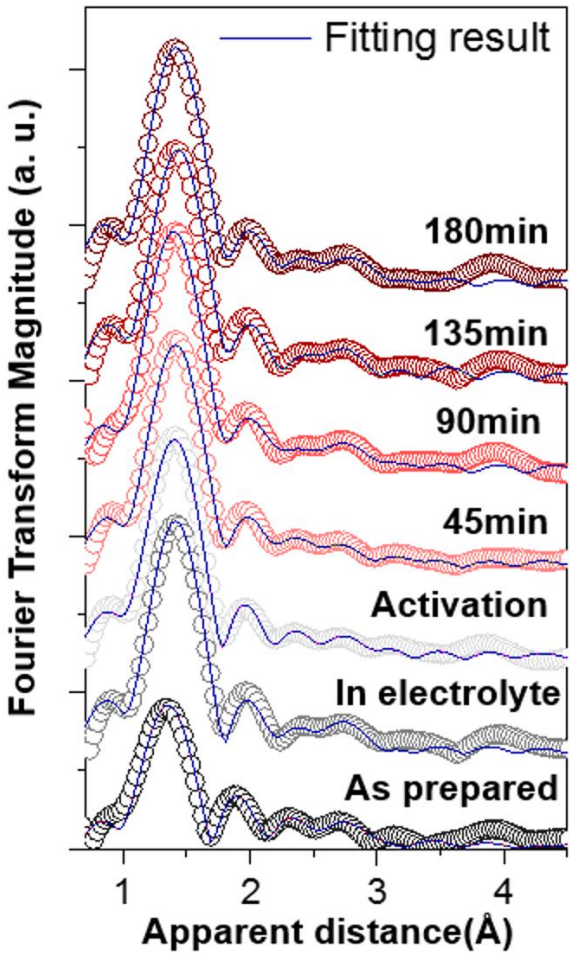

Figure S27. EXAFS r-space spectra of operando Co K-edge for Co-Fe-N-C sample (experimental data; color circle) and the corresponding fitting (red line). Fitting structural parameters are gathered in Table 1 and S3.

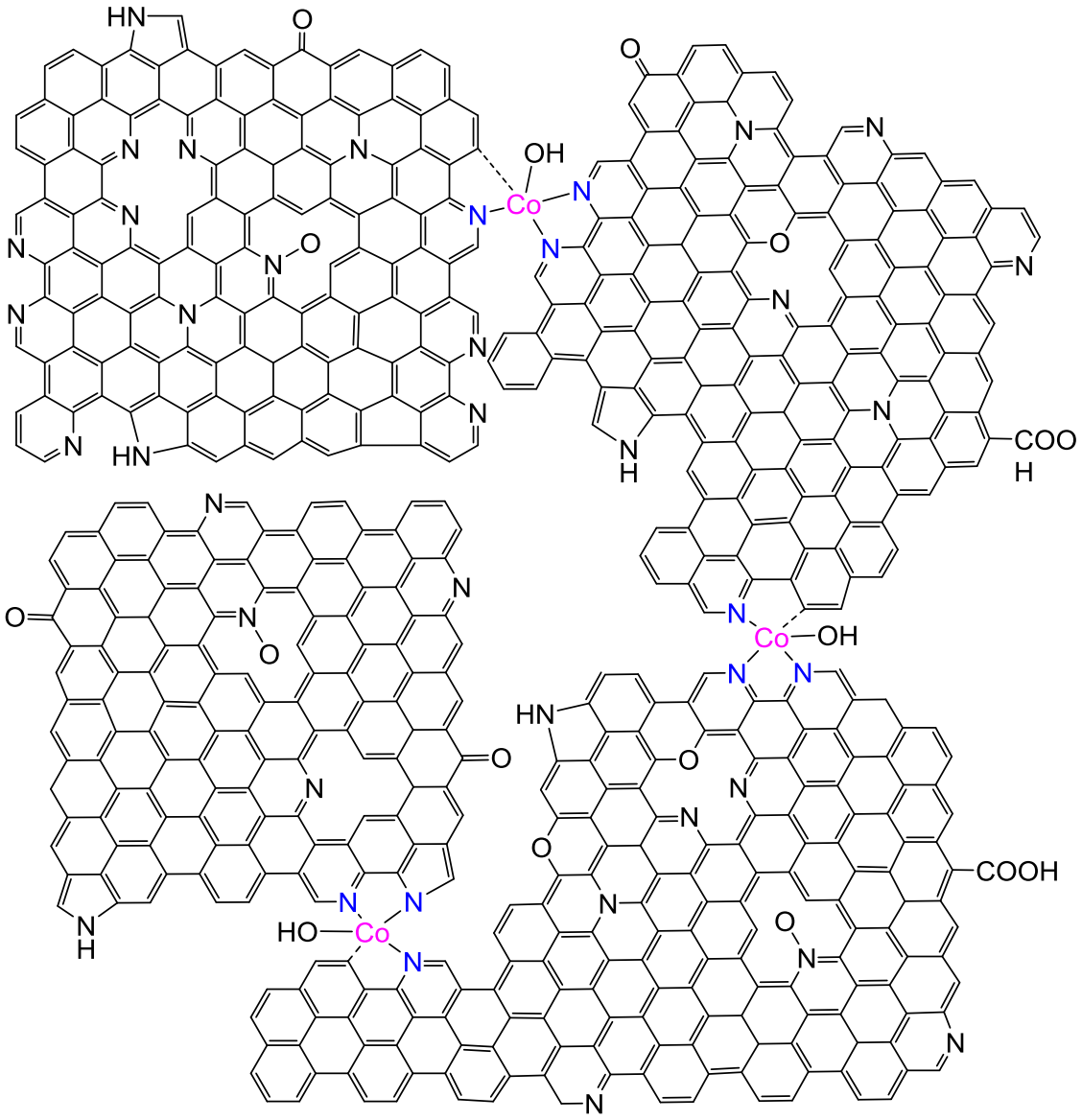

Figure S28. The proposed, indicative structure of the Co-N-C sample taking account of the results from the XAS study.

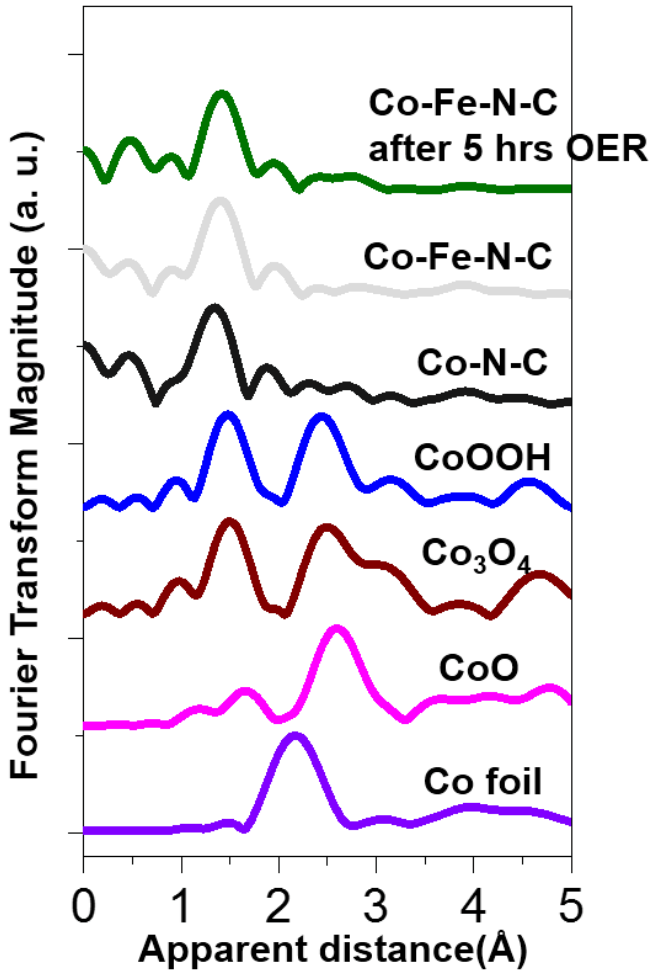

Figure S29. Fourier transform Co K-edge EXAFS spectra of as-prepared Co-N-C, Co-Fe-N-C (after activation) and Co-Fe-N-C after OER for 5 hours in comparison with Co reference samples.

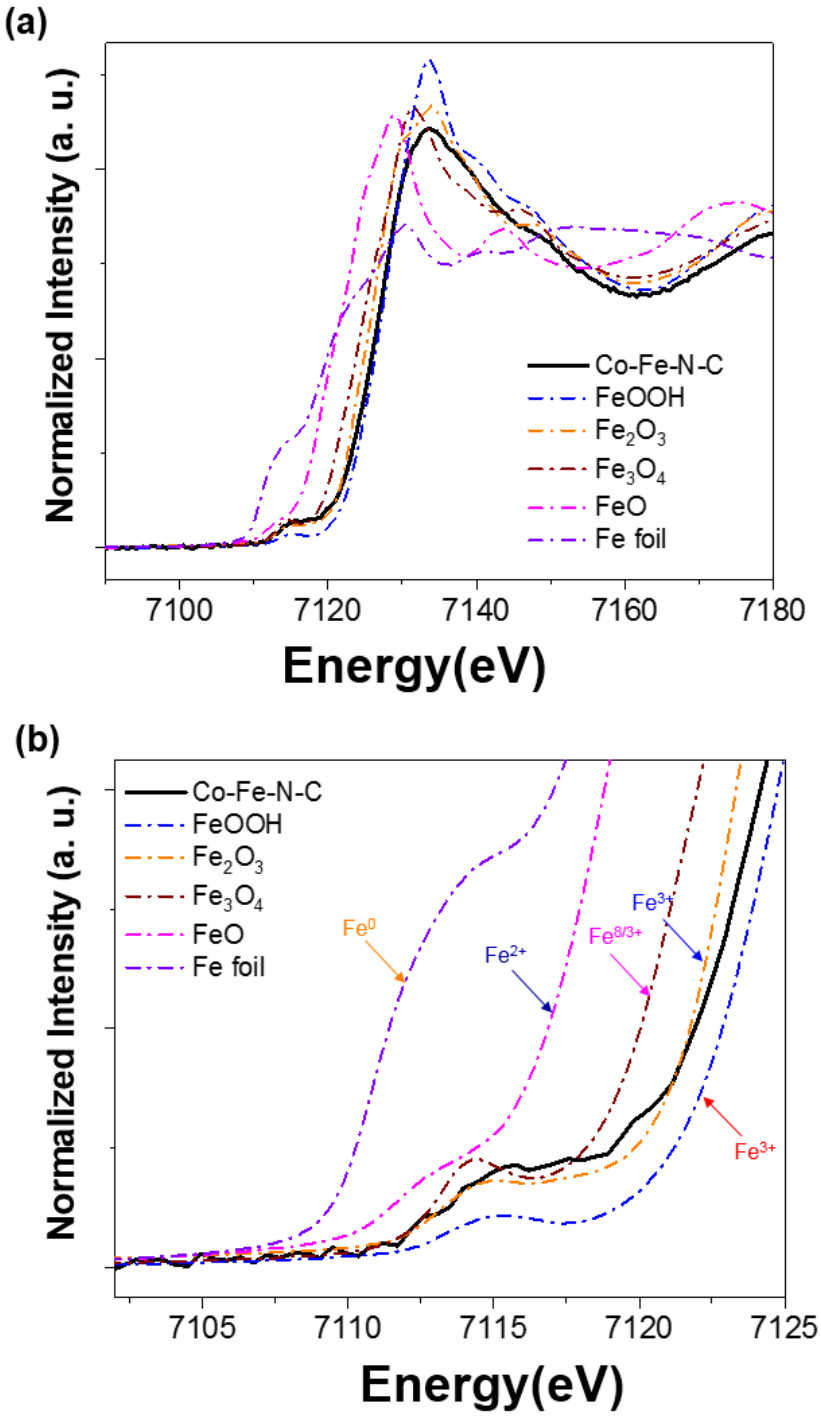

Figure S30. (a) XANES spectra of Fe K-edge for Co-Fe-N-C (after activation) and references including iron oxides and foil. (b) Magnified XANES for the transition from 1s to 4p.

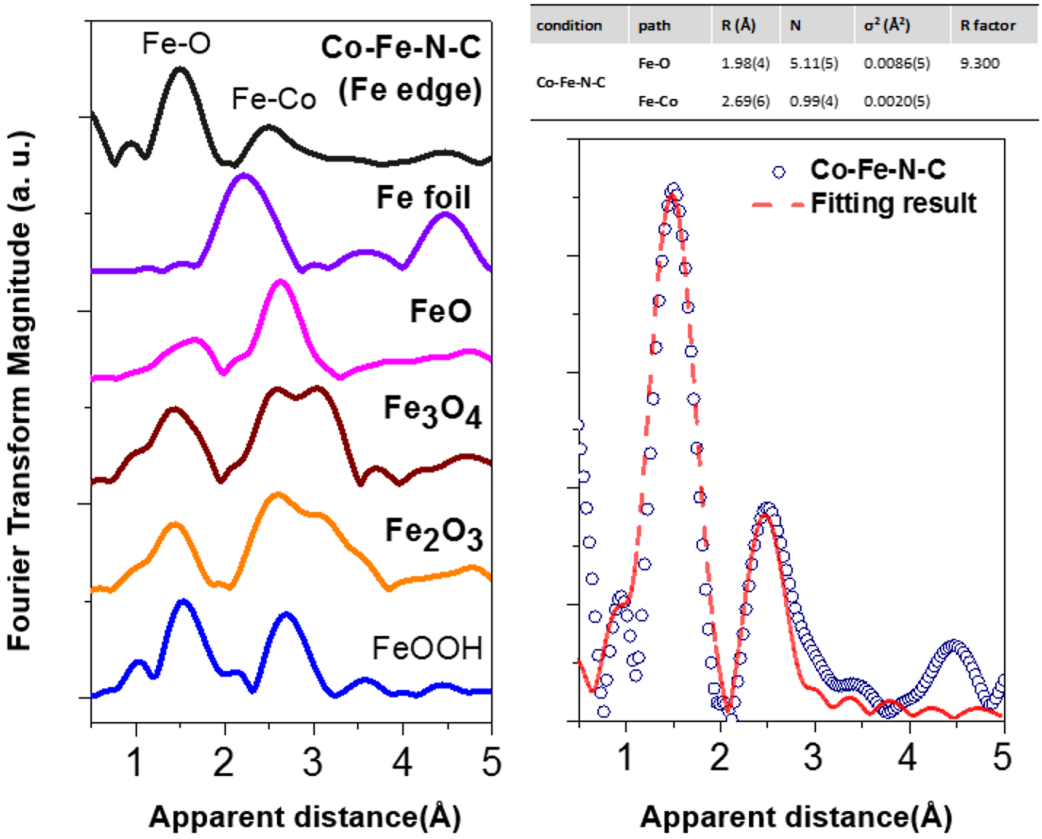

condition	path	R (Å)	N	σ^2 (Å^2)	R factor
Co-Fe-N-C	Fe-O	1.98(4)	5.11(5)	0.0086(5)	9.300
	Fe-Co	2.69(6)	0.99(4)	0.0020(5)	

Figure S31. EXAFS spectra of Fe K-edge for Co-Fe-N-C (after activation) and references including iron oxides and foil. EXAFS r-space spectra of Fe K-edge for Co-Fe-N-C sample (experimental data; color circle) and the corresponding fitting (red line). Fitting structural parameters are gathered in Table.

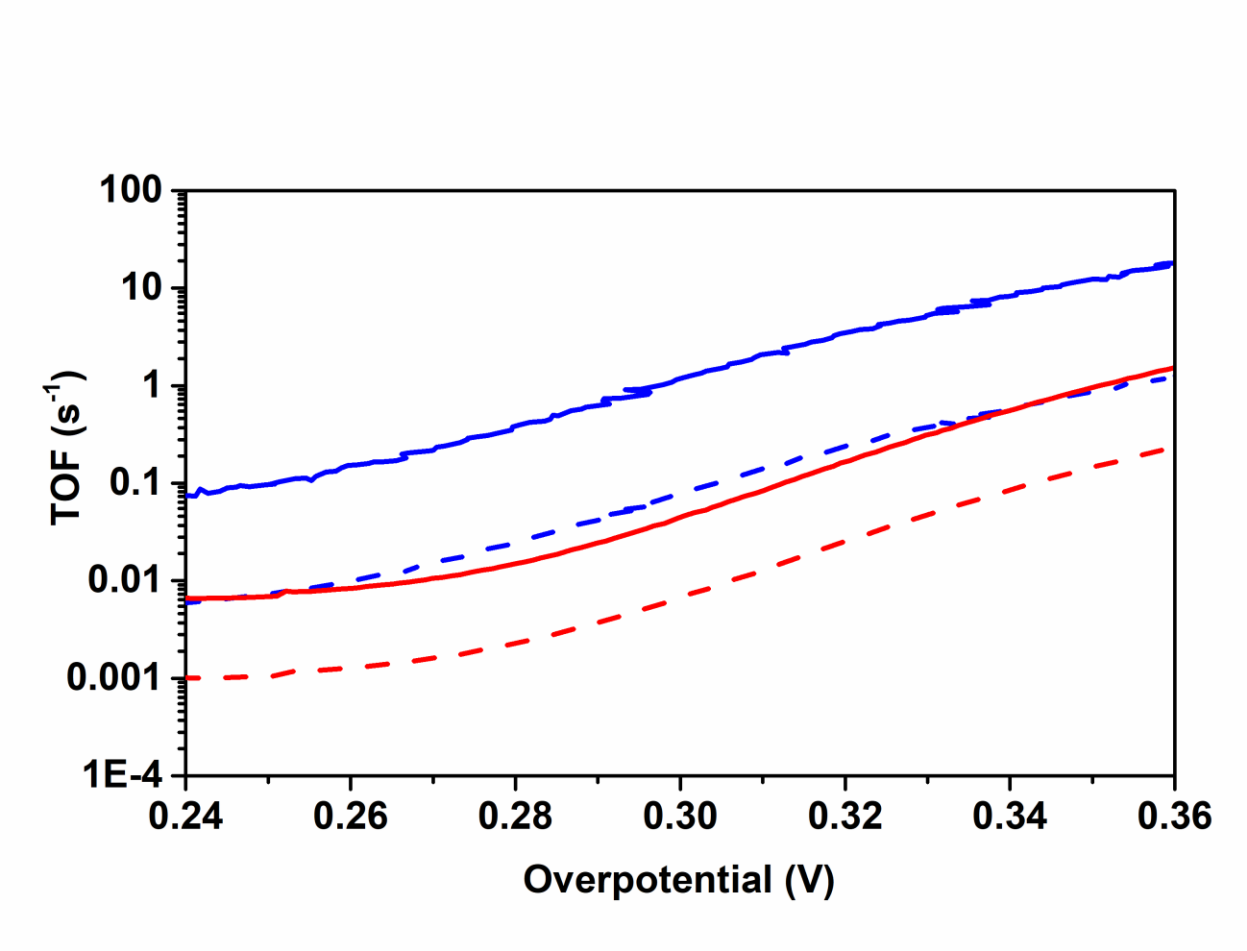

Figure S32. Potential-dependent TOFs of Co-Fe-N-C (blue curve) and activated Co-N-C-900 (in normal KOH, red curve). The solid lines are based on the loadings of dimetric Co-Fe sites and the dashed lines are based on the loadings of total metals (Co+Fe). The former represents the true activity while the latter is an indicative TOF.

Table S1. The performance of the activated Co-N-C (Co-Fe-N-C) modified on different electrode.

Type of the electrode	Overpotential @ 10 mA/cm^2 (mV)	Tafel Slope (mV/dec)
Glassy carbon	360 ± 8	44 ± 3
Carbon-cloth	321 ± 5	40 ± 2

Table S2. The performance of Co-N-C before and after activation in different KOH (1M).

	Overpotential @ 10 mA/cm^2 (mV)	Tafel Slope (mV/dec)
Before activation	495±19	72±4
Activated in Fe-free KOH	443±15	58±4
Activated in normal KOH	321±5	40±2
Activated in KOH with Fe (10 ppm)	309±4	37±2

Table S3. Structural parameters of Co-N-C and Co-Fe-N-C extracted from operando Co K-edge EXAFS refinement for as-prepared Co-N-C and after activation as well as under OER for various duration.

condition	path	R (Å)	N	σ^2 (Å^2)	R factor
As-prepared	**Co-C**	**1.59(6)**	**1.09(4)**	0.0096(8)	9.901
	Co-N	**1.87(4)**	**3.35(7)**	0.0087(4)	
	Co-O	**2.19(4)**	**0.74(6)**	0.0040(9)	
	Co-C1	2.90(5)	3.41(9)	0.0099(8)	
	Co-C2	3.19(4)	4.00(11)	0.0094(9)	
	Co-Fe	-	-	-	
In electrolyte	**Co-C**	**1.37(8)**	**0.41(5)**	0.0089(9)	3.926
	Co-N	**1.63(4)**	**1.52(5)**	0.0097(4)	
	Co-O	**1.87(4)**	**3.19(4)**	0.0054(4)	
	Co-C1	2.79(6)	2.30(5)	0.0073(9)	
	Co-C2	3.33(5)	2.19(8)	0.0076(5)	
	Co-Fe	-	-	-	
Activation	**Co-C**	**1.43(6)**	**0.46(6)**	0.0093(5)	3.191
	Co-N	**1.64(4)**	**1.51(6)**	0.0092(4)	
	Co-O	**1.83(6)**	**3.31(5)**	0.0061(4)	
	Co-C1	2.83(5)	2.21(7)	0.0074(8)	
	Co-C2	3.41(7)	2.10(8)	0.0084(9)	
	Co-Fe	2.51(4)	0.25(5)	0.0099(7)	
45 min	**Co-C**	**1.46(4)**	**0.47(4)**	0.0095(6)	2.883

	Co-N	**1.65(5)**	**1.51(6)**	0.0083(8)	
	Co-O	**1.84(4)**	**3.43(8)**	0.0064(4)	
	Co-C1	2.83(6)	2.27(6)	0.0091(9)	
	Co-C2	3.41(7)	2.17(8)	0.0097(9)	
	Co-Fe	2.61(5)	0.25(4)	0.0084(4)	
90 min	**Co-C**	**1.45(6)**	**0.43(4)**	0.0026(6)	4.034
	Co-N	**1.67(5)**	**1.53(4)**	0.0061(7)	
	Co-O	**1.87(4)**	**3.42(5)**	0.0050(4)	
	Co-C1	2.83(6)	2.28(6)	0.0053(7)	
	Co-C2	3.41(7)	2.15(7)	0.0046(9)	
	Co-Fe	2.63(7)	0.26(6)	0.0096(6)	
135 min	**Co-C**	**1.49(4)**	**0.45(1)**	0.0033(7)	4.015
	Co-N	**1.66(4)**	**1.54(6)**	0.0024(5)	
	Co-O	**1.85(5)**	**3.47(6)**	0.0053(4)	
	Co-C1	2.83(4)	2.24(6)	0.0038(6)	
	Co-C2	3.40(7)	2.17(8)	0.0073(9)	
	Co-Fe	2.63(5)	0.26(4)	0.0061(5)	
180 min	**Co-C**	**1.41(6)**	**0.45(4)**	0.0093(7)	3.043
	Co-N	**1.69(5)**	**1.54(4)**	0.0095(4)	
	Co-O	**1.86(4)**	**3.23(6)**	0.0048(4)	
	Co-C1	2.89(4)	2.14(5)	0.0083(7)	
	Co-C2	3.35(8)	2.10(8)	0.0066(9)	
	Co-Fe	2.71(4)	0.27(5)	0.0097(6)	

Table S4. Comparison of OER activity of Co-Fe-N-C with other OER catalysts based on nanomaterials based on 1st transition metals.

Catalysts	Electrolyte	Overpotential (mV) @ 10 mA/cm^2	Tafel slope (mV/dec)	TOF (s^{-1}) /overpotential (mV)	Reference
Co-N-C activated*	1 M KOH	321	40	12/350	**This work.**
CoOOH nanosheet	1 M KOH	300	38	0.09/340	[1]
Fe adsorbed CoO_x	1 M KOH	309	28	1.6/350	[2]
CoAl LDH-graphene	1 M KOH	252	36	1.14/350	[3]
FeO_x clusters on Ni foam	1M KOH	215	34	0.82/270	[4]
NiFe LDH-rGO	1 M KOH	207	39	0.99/300	[5]
NiFe LDH-CNT	1 M KOH	245	31	0.56/300	[6]
$NiFeO_x$	1 M KOH	297	37	1.9/300	[7]
Exfoliated NiFe LDH	1 M KOH	301	40	0.11/300	[8]
Plasma-assisted Exfoliated CoFe LDH	1 M KOH	267	38	4.78/300	[9]

* In a KOH adding with 10 ppm Fe(III), the overpotential is 309 mV (@10 mA/cm^2) while the Tafel slope is 37 mV/dec.

Table S5. Comparison of OER activity of Co-Fe-N-C with other single-atom catalysts and the catalysts based on sub-nano clusters.

Catalysts	Electrolyte	Overpotential (mV) @ 10 mA/cm^2	Tafel slope (mV/dec)	TOF (s^{-1}) /overpotential (mV)	Reference
Co-N-C activated*	1 M KOH	321	40	12/350	**This work.**
Co-g-C_3N_4-CNT	1 M KOH	370	62	-	[10]
Co-N,S-graphene	1 M KOH	370	62	0.27/350	[11]
Plasma treated ZIF-67	1 M KOH	319	70	0.082/320	[12]
Plasma treated ZIF-67	1 M KOH	310	54	0.462/300	[13]
Fe-N,S-CNT	1 M KOH	370	82	-	[14]
$Ni_4(PET)_8$	0.1 M KOH	330	38	-	[15]
$Ni_6(PET)_{12}$	0.1 M KOH	430	69	10/470	[16]
Ni-NHGF	1M KOH	331	63	0.72/300	[17]
Mn-GO	1 M KOH	337	55	-	[18]

* In a KOH adding with 10 ppm Fe(III), the overpotential is 309 mV (@10 mA/cm^2) while the Tafel slope is 37 mV/dec.

References

1. Huang, J.; Chen, J.; Yao, T.; He, J.; Jiang, S.; Sun, Z.; Liu, Q.; Cheng, W.; Hu, F.; Jiang, Y.; Pan, Z.; Wei, S., CoOOH Nanosheets with High Mass Activity for Water Oxidation. *Angew Chem Int Ed* **2015,** *54*, 8722-8727.
2. Gong, L.; Chng, X. Y. E.; Du, Y.; Xi, S.; Yeo, B. S., Enhanced Catalysis of the Electrochemical Oxygen Evolution Reaction by Iron(III) Ions Adsorbed on Amorphous Cobalt Oxide. *ACS Catal* **2018,** *8*, 807-814.
3. Ping, J.; Wang, Y.; Lu, Q.; Chen, B.; Chen, J.; Huang, Y.; Ma, Q.; Tan, C.; Yang, J.; Cao, X.; Wang, Z.; Wu, J.; Ying, Y.; Zhang, H., Self-Assembly of Single-Layer CoAl-Layered Double Hydroxide Nanosheets on 3D Graphene Network Used as Highly Efficient Electrocatalyst for Oxygen Evolution Reaction. *Adv Mater* **2016,** *28*, 7640-7645.
4. Song, F.; Busch, M. M.; Lassalle-Kaiser, B.; Hsu, C.-S.; Petkucheva, E.; Bensimon, M.; Chen, H. M.; Corminboeuf, C.; Hu, X., An Unconventional Iron Nickel Catalyst for the Oxygen Evolution Reaction. *ACS Cent. Sci.* **2019,** *5*, 558-568.
5. Long, X.; Li, J.; Xiao, S.; Yan, K.; Wang, Z.; Chen, H.; Yang, S., A strongly coupled graphene and FeNi double hydroxide hybrid as an excellent electrocatalyst for the oxygen evolution reaction. *Angew Chem Int Ed* **2014,** *53*, 7584-7588.
6. Gong, M.; Li, Y.; Wang, H.; Liang, Y.; Wu, J. Z.; Zhou, J.; Wang, J.; Regier, T.; Wei, F.; Dai, H., An advanced Ni-Fe layered double hydroxide electrocatalyst for water oxidation. *J Am Chem Soc* **2013,** *135*, 8452-8455.
7. Fominykh, K.; Chernev, P.; Zaharieva, I.; Sicklinger, J.; Stefanic, G.; Doblinger, M.; Muller, A.; Pokharel, A.; Bocklein, S.; Scheu, C.; Bein, T.; Fattakhova-Rohlfing, D., Iron-doped nickel oxide nanocrystals as highly efficient electrocatalysts for alkaline water splitting. *ACS Nano* **2015,** *9*, 5180-5188.
8. Song, F.; Hu, X., Exfoliation of layered double hydroxides for enhanced oxygen evolution catalysis. *Nat Commun* **2014,** *5*, 4477.
9. Wang, Y.; Zhang, Y.; Liu, Z.; Xie, C.; Feng, S.; Liu, D.; Shao, M.; Wang, S., Layered Double Hydroxide Nanosheets with Multiple Vacancies Obtained by Dry Exfoliation as Highly Efficient Oxygen Evolution Electrocatalysts. *Angew Chem Int Ed* **2017,** *56*, 5867-5871.
10. Zheng, Y.; Jiao, Y.; Zhu, Y.; Cai, Q.; Vasileff, A.; Li, L. H.; Han, Y.; Chen, Y.; Qiao, S. Z., Molecule-Level g-C3N4 Coordinated Transition Metals as a New Class of Electrocatalysts for Oxygen Electrode Reactions. *J Am Chem Soc* **2017,** *139*, 3336-3339.
11. Wang, J.; Ge, X.; Liu, Z.; Thia, L.; Yan, Y.; Xiao, W.; Wang, X., Heterogeneous Electrocatalyst with Molecular Cobalt Ions Serving as the Center of Active Sites. *J Am Chem Soc* **2017,** *139*, 1878-1884.
12. Dou, S.; Dong, C.-L.; Hu, Z.; Huang, Y.-C.; Chen, J.-l.; Tao, L.; Yan, D.; Chen, D.; Shen, S.; Chou, S.; Wang, S., Atomic-Scale CoOx Species in Metal-Organic Frameworks for Oxygen Evolution Reaction. *Adv Funct Mater* **2017,** *27*, 1702546.
13. Tao, L.; Lin, C.-Y.; Dou, S.; Feng, S.; Chen, D.; Liu, D.; Huo, J.; Xia, Z.; Wang, S., Creating coordinatively unsaturated metal sites in metal-organic-frameworks as efficient electrocatalysts for the oxygen evolution reaction: Insights into the active centers. *Nano Energy* **2017,** *41*, 417-425.
14. Chen, P.; Zhou, T.; Xing, L.; Xu, K.; Tong, Y.; Xie, H.; Zhang, L.; Yan, W.; Chu, W.; Wu, C.; Xie, Y., Atomically Dispersed Iron-Nitrogen Species as Electrocatalysts for Bifunctional Oxygen Evolution and Reduction Reactions. *Angew Chem Int Ed* **2017,** *56*, 610-614.
15. Joya, K. S.; Sinatra, L.; AbdulHalim, L. G.; Joshi, C. P.; Hedhili, M. N.; Bakr, O. M.; Hussain, I., Atomically monodisperse nickel nanoclusters as highly active electrocatalysts for water oxidation. *Nanoscale* **2016,** *8*, 9695-9703.
16. Kauffman, D. R.; Alfonso, D.; Tafen, D. N.; Lekse, J.; Wang, C.; Deng, X.; Lee, J.; Jang, H.; Lee, J.-s.; Kumar, S.; Matranga, C., Electrocatalytic Oxygen Evolution with an Atomically Precise Nickel Catalyst. *ACS Catal* **2016,** *6*, 1225-1234.

17. Fei, H.; Dong, J.; Feng, Y.; Allen, C. S.; Wan, C.; Volosskiy, B.; Li, M.; Zhao, Z.; Wang, Y.; Sun, H.; An, P.; Chen, W.; Guo, Z.; Lee, C.; Chen, D.; Shakir, I.; Liu, M.; Hu, T.; Li, Y.; Kirkland, A. I.; Duan, X.; Huang, Y., General synthesis and definitive structural identification of MN4C4 single-atom catalysts with tunable electrocatalytic activities. *Nat Catal* **2018,** *1*, 63-72.
18. Guan, J.; Duan, Z.; Zhang, F.; Kelly, S. D.; Si, R.; Dupuis, M.; Huang, Q.; Chen, J. Q.; Tang, C.; Li, C., Water oxidation on a mononuclear manganese heterogeneous catalyst. *Nat Catal* **2018,** *1*, 870-877.